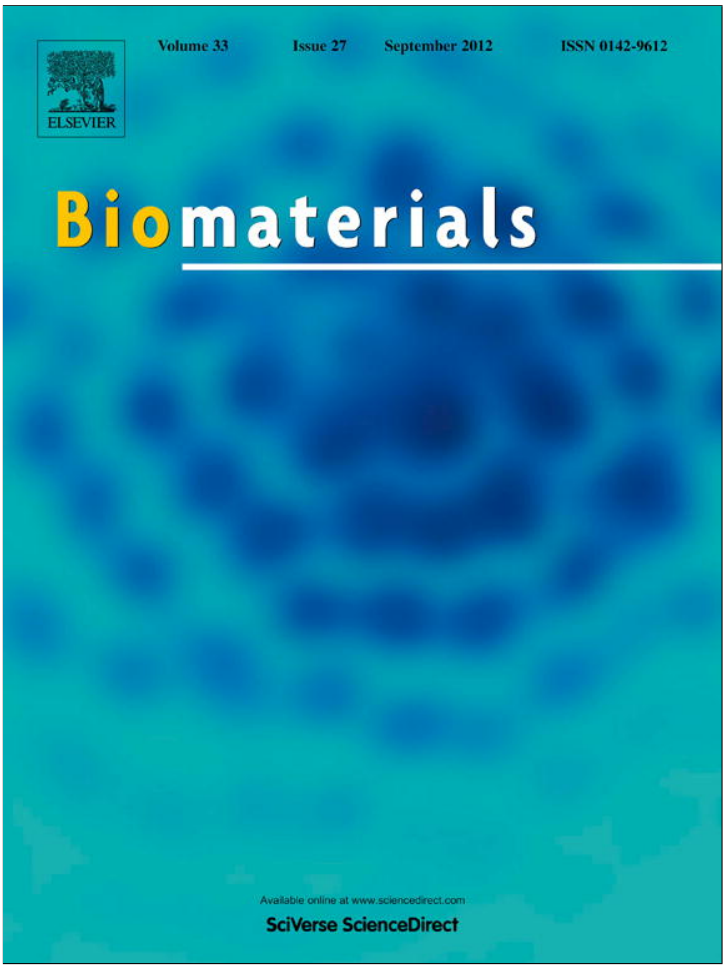

Biomaterials 33 (2012) 6456–6467

Contents lists available at SciVerse ScienceDirect

Biomaterials

journal homepage: www.elsevier.com/locate/biomaterials

A reverse complementary multimodal imaging system to visualize microRNA9-involved neurogenesis using peptide targeting transferrin receptor-conjugated magnetic fluorescence nanoparticles

Mi-hee Jo [a], Bahy A. Ali [b,e], Abdulaziz A. Al-Khedhairy [b], Chang Hyun Lee [a], Bongjune Kim [c], Seungjoo Haam [c], Yong-Min Huh [d], Hae Young Ko [a], Soonhag Kim [a,*]

[a] Laboratory of Molecular Imaging, Department of Biomedical Science, CHA University, 605-21 Yoeksam 1-dong, Gangnam-gu, Seoul 135-081, South Korea
[b] Department of Zoology, College of Science, King Saud University, Riyadh 11451, Saudi Arabia
[c] Department of Chemical and Biomolecular Engineering, Yonsei University, Seoul 120-749, South Korea
[d] Department of Radiology, College of Medicine, Yonsei University, Seoul 120-752, South Korea
[e] Department of Nucleic Acids Research, Genetic Engineering and Biotechnology Research Institute, City for Scientific Research and Technology Applications, Alexandria, Egypt

ARTICLE INFO

Article history:
Received 21 May 2012
Accepted 27 May 2012
Available online 23 June 2012

Keywords:
MicroRNA
Multimodal imaging
MR imaging
Nanoparticle
Transferrin receptor
Neuronal differentiation

ABSTRACT

Multimodal imaging systems may eliminate the disadvantages of individual imaging modality by providing complementary information about cellular and molecular activites. In this sutdy, we developed a reverse complementary multimodal imaging system to image microRNAs (miRNA, miR) during neurognesis using transferrin receptor (TfR) and a magnetic fluorescence (MF) nanoparticle-conjugated peptide targeting TfR (MF targeting TfR). Both *in vitro* and *in vivo* imaging demonstrated that, in the absence of miR9 during pre-differentiation of P19 cells, the MF targeting TfR nanoparticles greatly targeted TfR and were successfully internalized into P19 cells, resulting in high fluorescence and low MR signals. When the miR9 was highly expressed during neurogenesis of P19 cells, the MF targeting TfR nanoparticles were hardly targeted due to the miR9 function, which represses the expression and functional activity of TfR from the miRNA TfR reproter gene, resulting in low fluorescence and high MR signals. The reverse complementary multimodal miRNA imaging system may serve as a new imaging probe to montior miRNA-involved cellular developments and diseases.

1. Introduction

MicroRNAs (miRNA, miR) are a class of small endogenous non-coding RNAs that negatively regulate gene expression of protein-coding genes in animals and plants [1,2]. It is well-known that miRNA functions are associated with a wide variety of cellular activities, including fat metabolism, apoptosis, cellular differentiation and proliferation as well as clinically important diseases [3–12]. Several miRNAs, including miR124a, miR9, miR9*, miR128, miR23a, miR132 and miR134, have recently been found in neurons and shown to regulate neuronal development [13,14]. Among them, miR9 is specifically expressed in the brain and abundant in neurogenic regions in embryos and adults [15,16].

To date, most of the current methods to detect the expression of endogenous miRNAs, including northern blot analysis, microarray and quantitative real-time polymerase chain reaction (qRT-PCR) are invasive and only investigate a predefined two-dimensional plane [14,17]. According to the theory of sequence-based hybridization of miRNA with its target mRNA, our group has successfully developed two different non-invasive miRNA imaging methods using a bioluminescent luciferase reporter gene and a fluorescent molecular beacon to visualize miRNA biogenesis and understand miRNA function in intact cells and living organisms during neurogenesis, myogenesis and carcinogenesis [16–23]. However, there are a few of concerns in regards to both miRNA imaging systems. The bioluminescent miRNA reporter gene, which contains perfectly complementary sequences of mature miRNAs in the 3′ untranslated region (UTR) of the luciferase, is a signal-off system in the presence of miRNAs, since the miRNA destabilizes its target mRNA. This signal-off miRNA imaging system may have limitations in regards to differentiating the decreased bioluminescent signals from miRNA expression or cellular loss. The fluorescent miRNA molecular beacon, which is composed of oligonucleotides complementary to miRNAs and fluorophore–quencher pairs, successfully overcome the limitation of the bioluminescent miRNA reporter gene by providing signal-on data in the presence of miRNAs. However, both miRNA imaging systems are still not readily adaptable to clinical

* Corresponding author. Tel.: +82 2 555 5063; fax: +82 2 3468 3373.
E-mail address: kimsoonhag@empal.com (S. Kim).

0142-9612/$ – see front matter © 2012 Elsevier Ltd. All rights reserved.
doi:10.1016/j.biomaterials.2012.05.057

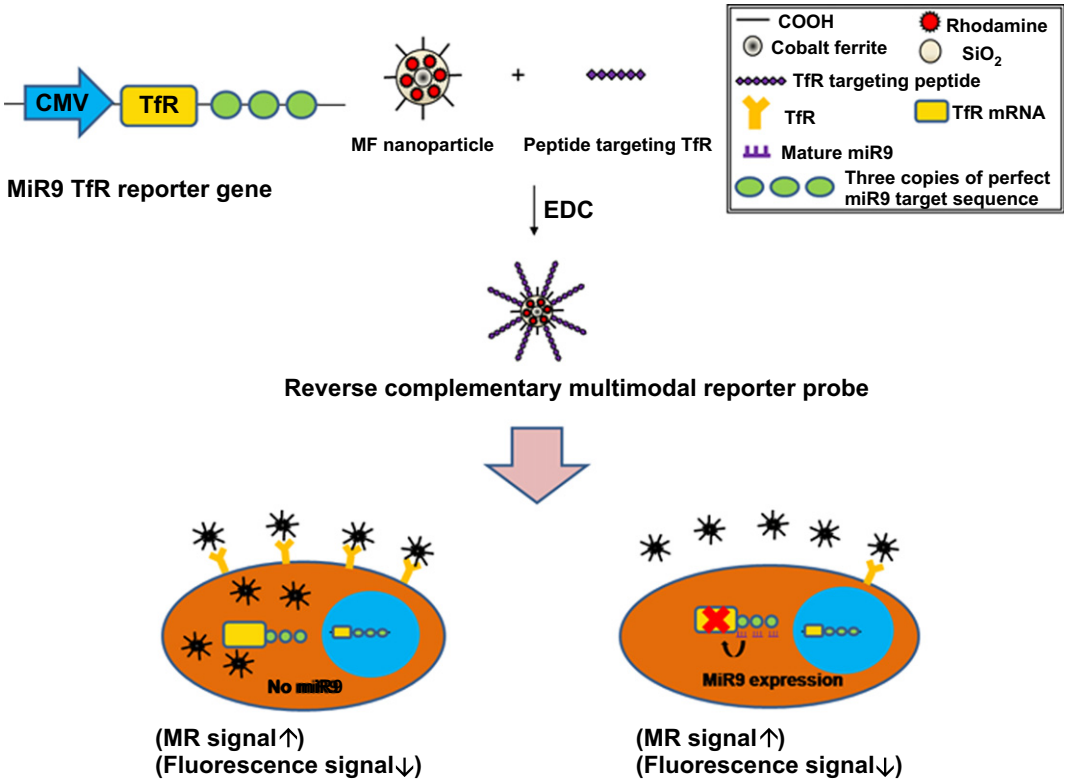

Fig. 1. Schematic of the reverse complementary multimodal imaging system.

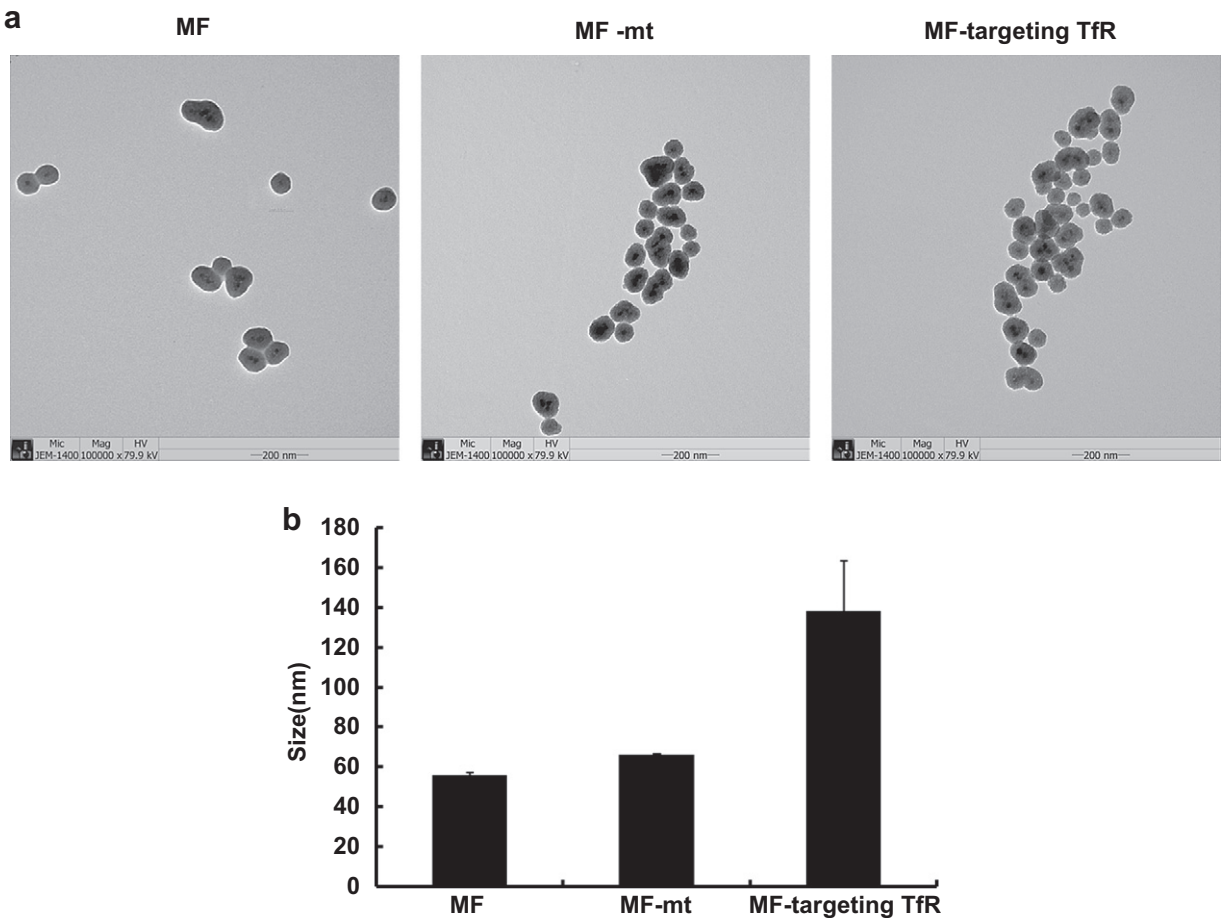

Fig. 2. Morphology characteristics of the reverse complementary multimodal reporter probe. (a) TEM images of MF, MF-mt and MF targeting TfR. Scale bars represent 200 nm (b) DLS analysis of MF, MF-mt and MF targeting TfR.

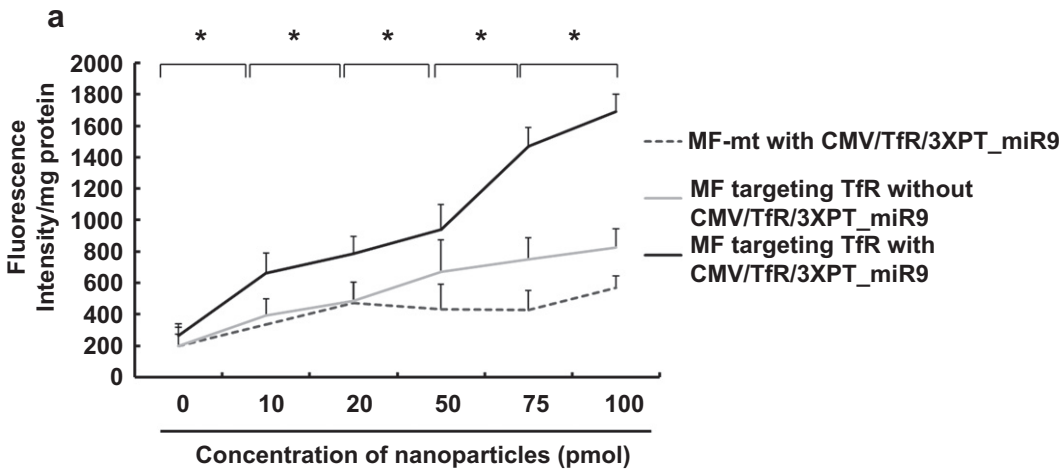

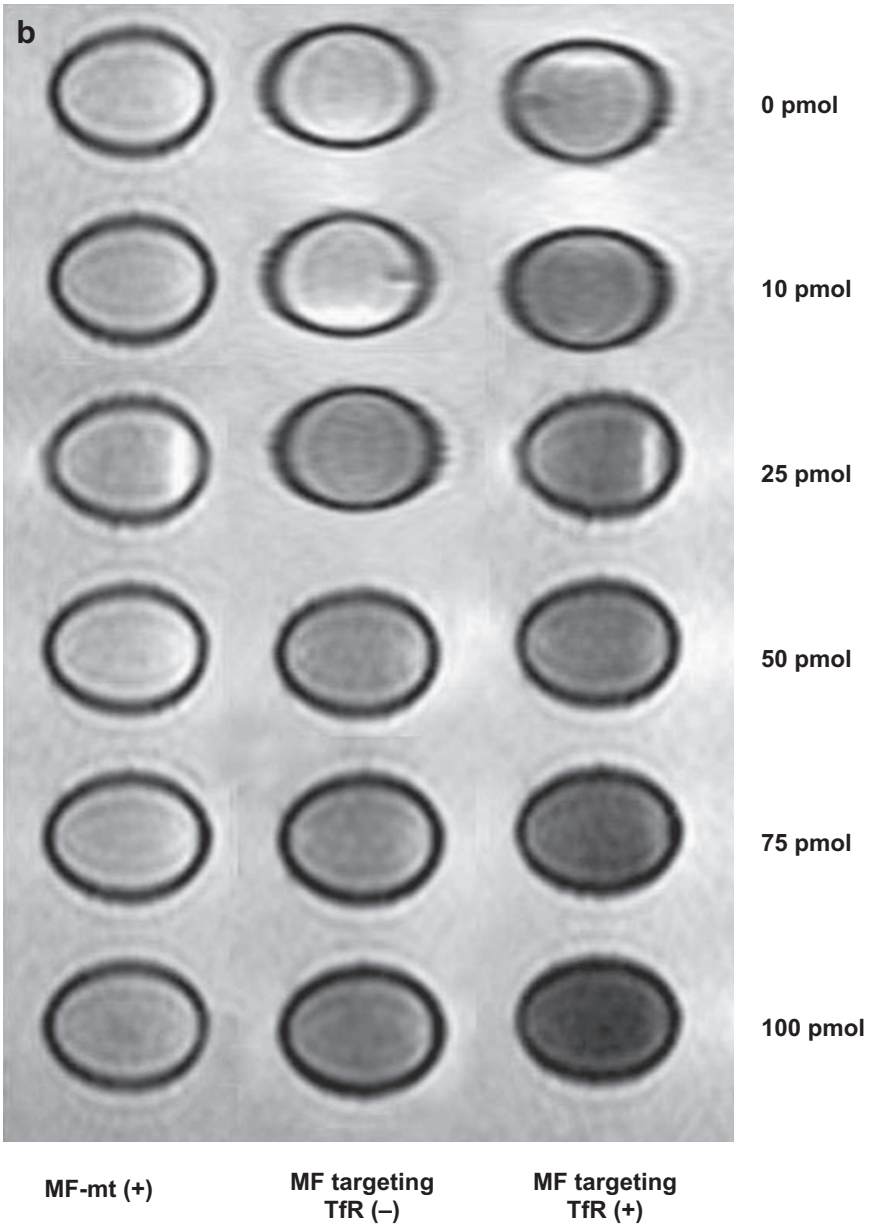

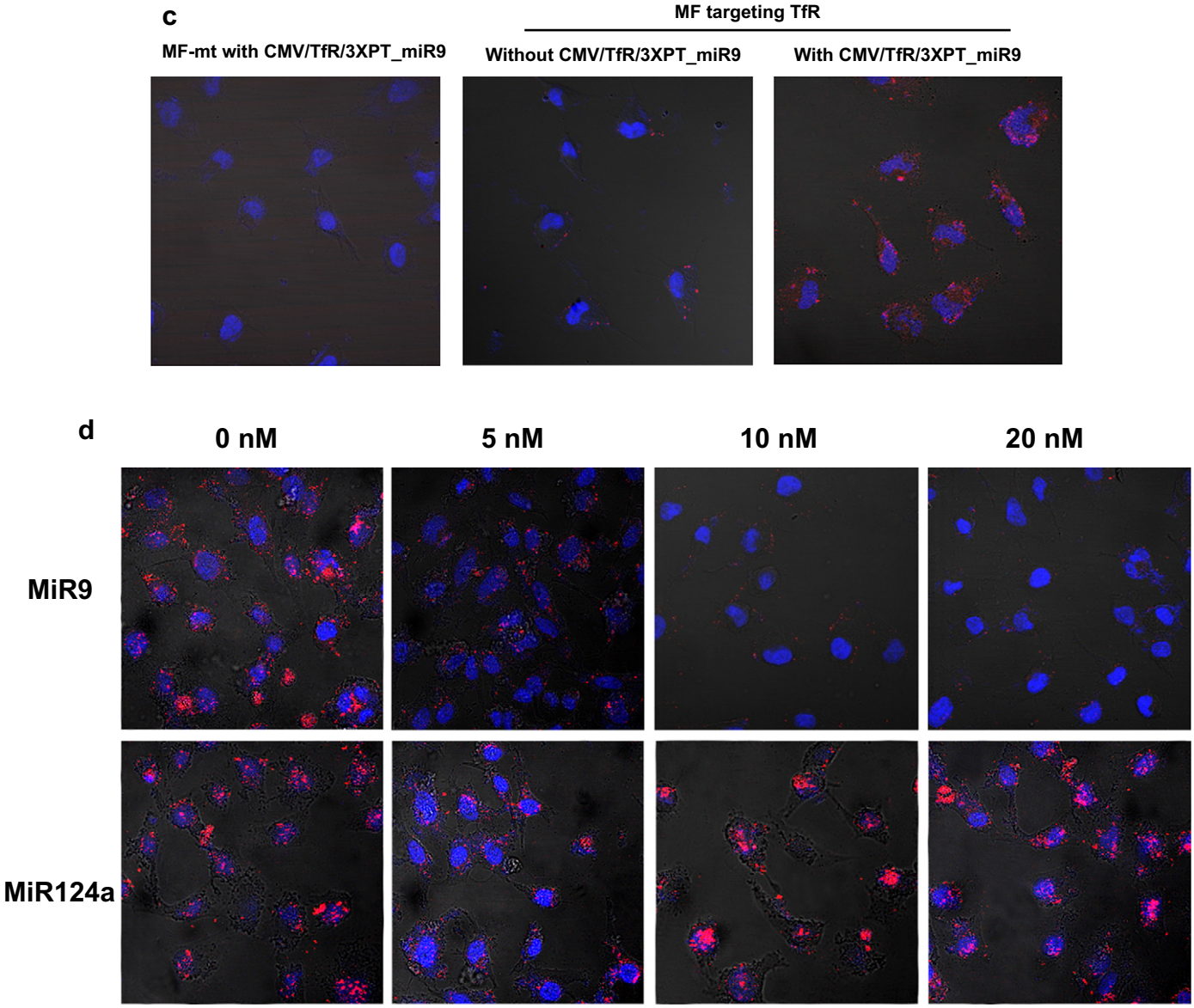

Fig. 3. (*continued*).

application due to the attenuation of optical signals in deep tissue and organs. The development of multimodal signal-on miRNA imaging systems with more clinically relevant imaging modalities, such like radioisotope and magnetic resonance (MR) imaging is required for clinical application of imaging miRNAs.

MR imaging (MRI) provides exquisite spatial resolution for deep tissues and anatomic and physiological information [24–26]. A number of nanoparticle-based MRI have been developed and used in stem cell tracking by *ex vivo* labeling of the cells with superparamagnetic nanoparticles [27,28]. However, this method cannot be used to monitor gene expression-based cellular development processes, including differentiation and apoptosis. Recently, MRI reporter genes, transferrin receptor (TfR) and ferritin, have been developed and provides gene expression with anatomic and functional imaging information [26,29–31]. A MRI reporter gene that can provide serial temporal imaging from the same animal might be useful for imaging gene expression-based cellular development processes.

In this study, we developed a new approach for imaging miRNA-involved cellular development processes using a multimodal nanoparticle-based reverse complementary imaging system. In this system, miR9 was selected for imaging neurogenesis and the TfR gene was utilized as a miRNA reporter gene. For targeting TfR and reporting reverse complementary multimodal imaging information, peptide targeting TfR, which is a 12-mer peptide sequence that binds to TfR and is internalized via endocytosis into TfR-expressing cells [32], was conjugated to magnetic fluorescence

Fig. 3. Specificity of the reverse complementary multimodal imaging system in HeLa cells. (a, b, c) Fluorescence intensity, T2-weighted MR image and confocal microscopy image of the reverse complementary multimodal imaging system in the absence of miR9 in HeLa cells. Various concentrations of the MF targeting TfR or the MF-mt nanoparticles were treated into HeLa cells transfected either with (+) or without (−) the CMV/TfR/3XPT_miR9. (d, e, f) Confocal microscopy images, T2-weighted MR image and fluorescence intensity of the reverse complementary multimodal imaging system in the presence of miR9 in HeLa cells. HeLa cells transfected with the CMV/TfR/3XPT_miR9 were treated with various concentrations (0, 5, 10 and 20 nM) of either miR9 or miR124a (used as a control) and with 30 pmol of the MF targeting TfR nanoparticles. Data are displayed as means ± standard deviation ($^{*}P < 0.05$, $^{**}P < 0.005$). RITC image (red, X400) of each nanoparticle was acquired at an excitation of 555 nm and emission of 578 nm. All confocal images were merged with the 4′, 6-diamidino-2-phenylindole (DAPI) image (nucleus staining, 460 nm) and cellular morphology.

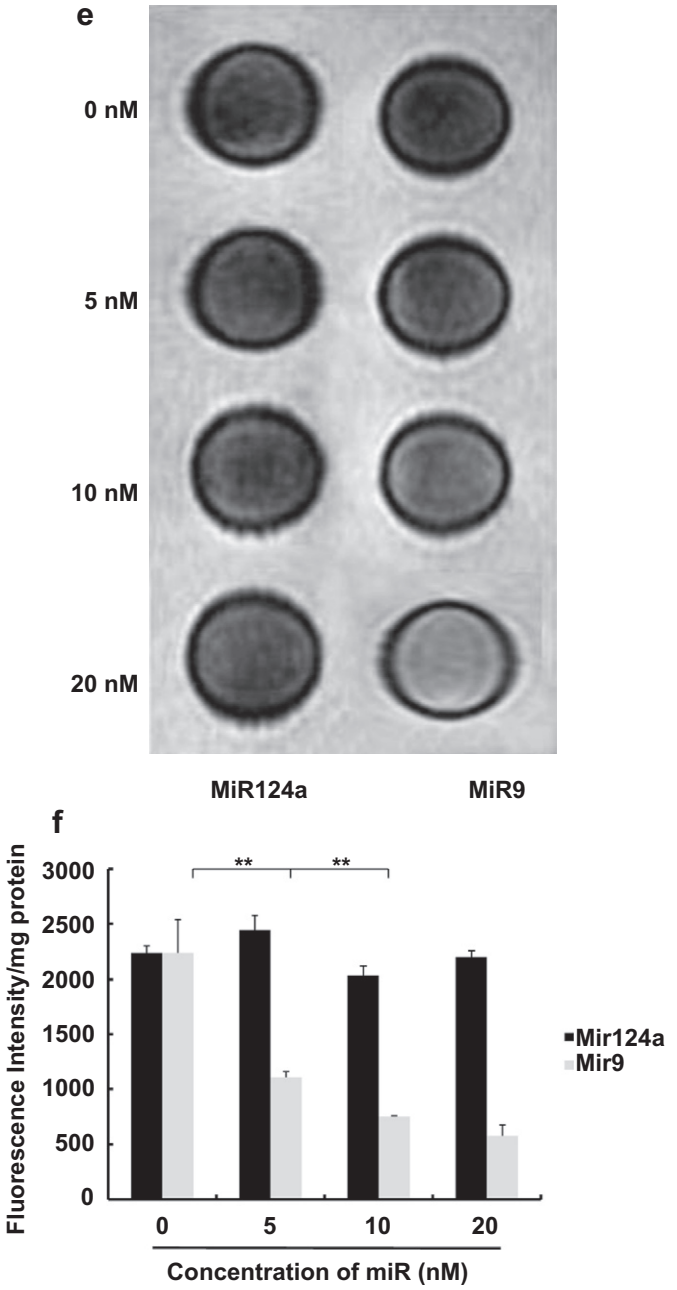

Fig. 3. (*continued*).

(MF) nanoparticles consisting of a cobalt ferrite core coated with a silica shell that contained Rhodamine B isothicyanate (RITC, Excitation/Emission = 555/578 nm) [23,33]

2. Materials and methods

2.1. Construction of the miR9 TfR reporter gene

DNA fragment encoding TfRgene were inserted between XhoI and EcoRI of pDsRed2-N1 vector (Clontech, Palo Alto, CA) to cunstruct the TfR reporter vector (CMV/TfR). The nucleotide sequences of mature miR9 were obtained from the miRNAMap database (http://mirnamap.mbc.nctu.edu.tw) and we constructed 3 copies of a perfect complementary target sequence of mature miR9 (3XPT_miR9) by annealing the following oligonucleotides: 5′-CGTTCATACAGCTAGATAACCAAAGAT AGTATCATACAGCTAGATAACCAAA GATAGTATCATACAGCTAGATAACCAAAGAG-3′, 5′-GATCCTCTTTGGTTATCTAG CTGTATGATACTATCTTTGGTTATCTAGCTGTATGATACTAT CTTTGGTTATCTAGCTGTATGAACGGTC-3′. The miR9 TfR reporter vector was designed by inserting three copies of a perfectly complementary miR9 target sequence into the *KpnI* and *BamHI* site of CMV/TfR (designed as CMV/TfR/3XPT_miR9). Three copies of perfect targets before the poly (A) tail enhanced the response of CMV/TfR to the repressive activity of mature miR9.

2.2. Construction of the reverse complementary multimodal reporter probe

MNP@SiO_2(RITC)-PEG/COOH nanoparticles (MF, 2 mg/mL) were purchased from Biterials (Seoul, Korea) and peptides targeting TfR (H-Thr-His-Arg-Pro-Pro-Met-Trp-Ser-Pro-Val-Trp-Pro-OH) were purchased from ANASPEC (Fremont, CA). MF particles were covalently linked to the peptide using *N*-(3-dimethylaminopropyl)-*N*-ethylcarbodimide (EDC) (MF: TfR targeting peptide molar ratio in conjugation reaction, 1:3) (Sigma, Saint Louis, MO) for 1 h at room temperature to synthesize the reverse complementary multimodal reporter probe (MF targeting TfR). The MF targeting TfR nanoparticles were washed off by centrifugation at 22,250 g for 10 min and resuspended in selection buffer solution (50 mM Tris–HCl, pH7.4) after 1 h of incubation. After each conjugation, the distribution and size of the MF targeting TfR were analyzed by TEM using a JEM 1010 system (JEOL, Japan) and DLS using a Zetasizer Nano ZS system (Malvern Instruments, Worcestershire, UK).

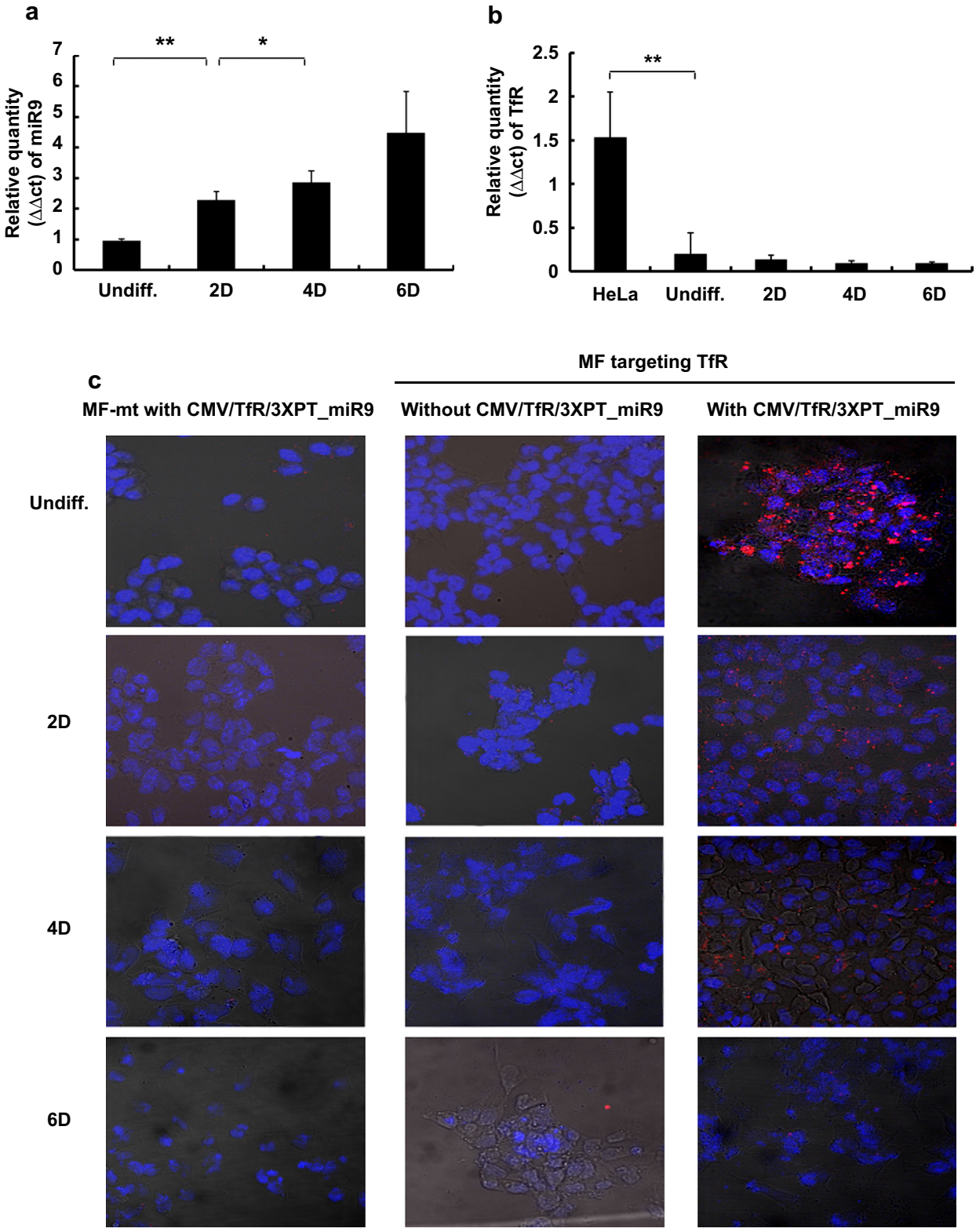

Fig. 4. *In vitro* analysis of the reverse complementary multimodal imaging system in P19 cells. (a, b) Real-time PCR for miR9 and TfR expression before (undifferentiation, Undiff.) and 2 days, 4 days and 6 days after neuronal differentiation of P19 cells. HeLa cells for TfR expression were used as a control. Data are displayed as means ± standard deviation ($^{*}P < 0.05$, $^{**}P < 0.005$). (c, d, e) Confocal microscopy image, fluorescence intensity and T2-weighted MR image of the reverse complementary multimodal imaging system during neurogenesis of P19 cells. Undifferentiated and 2-day-, 4-day- and 6-day after differentiation of P19 cells transfected either with (+) or without (−) the CMV/TfR/3XPT_miR9 were treated with 30 pmol of the MF targeting TfR nanoparticles or 30 pmol of the MF-mt nanoparticles. RITC image (red, X400) of each nanoparticle was acquired at excitation of 555 nm and emission of 578 nm. All confocal images were merged with the 4′, 6-diamidino-2-phenylindole (DAPI) image (nucleus staining, 460 nm) and cellular morphology. Data are displayed as means ± standard deviation ($^{*}P < 0.05$, $^{**}P < 0.005$).

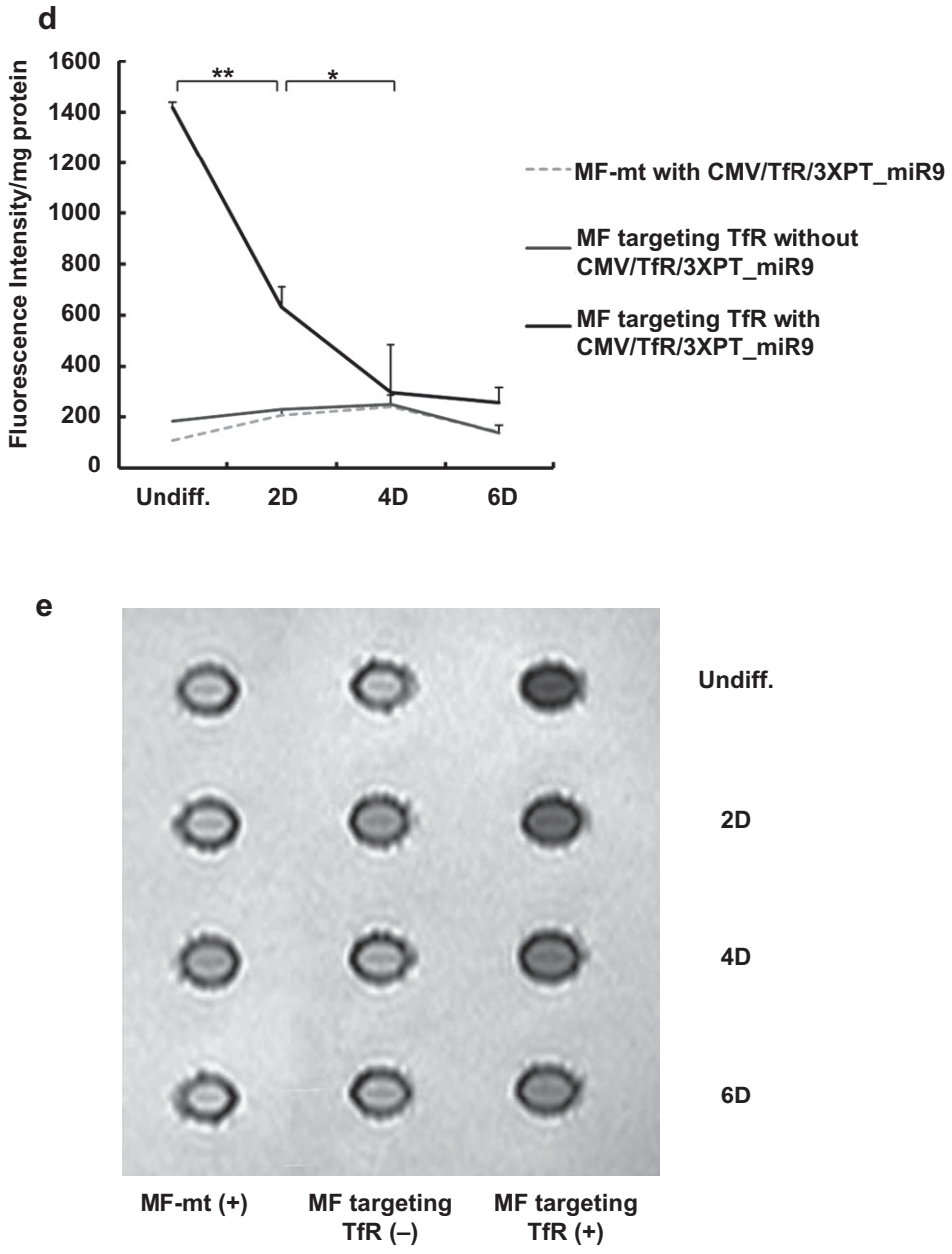

Fig. 4. (*continued*).

2.3. Cell culture and transfection

HeLa cells (human cervical cancer cell line) and P19 cells (mouse embryonic teratocarcinoma cell lines) were used to evaluate the specificity of the miR9 TfR reporter gene-based reverse complementary multimodal imaging system. HeLa cells were cultured in Dulbecco's Modified Eagle Medium (DMEM, Invitrogen, Grand Island, NY) containing 10% fetal bovine serum (FBS, Grand Island, NY) and 1% antibiotics (Invitrogen, Grand Island, NY); this was passaged to 70–80% confluence. The P19 cells were maintained in minimal essential medium-alpha (a-MEM, Gibco, Grand Island, NY) containing 7.5% bovine calf serum (BS, Gibco, USA), 2.5% FBS and 1% antibiotics in a 5% CO_2-humidified chamber. For the induction of neuronal differentiation, DMEM/F12 (1:1) medium (Gibco, Grand Island, NY) containing 1% insulin–transferrin–selenium (ITS, Gibco, Grand Island, NY), 1% antibiotics and 0.5 μM all-trans-retinoic acid (RA Sigma, St Louis, MO) were used. The P19 differentiation medium was replaced with new RA-containing differentiation medium every 2 days. To image miR9 during neuronal differentiation in the P19 cells, which was induced by treatment with RA, the plate was coated with autoclaved 0.1% gelatin solution (Sigma, St Louis, MO). The HeLa and P19 cells were transiently transfected with precursor miR9 (Ambion, Austin, TX) and/or the miR9 TfR reporter gene using Lipofectamine and the Plus reagent (Invitrogen, Grand Island, NY). All of the transient transfections were carried out in triplicate.

2.4. Real-time PCR

Using Trizol reagent (Invitrogen, Grand Island, NY), total RNA was isolated from HeLa and P19 cells the day after RA treatment. Reverse transcription, which was performed to synthesize the first-strand cDNA, was carried out using random-hexamer and SuperScript II reverse transcriptase (Invitrogen, Grand Island, NY). Quantitative real-time PCR (qRT-PCR) primer set for TfR expression was as follows: 5′-GCAGGGAAAATCACCTTTG-3′ (TfR forward) and 5′-GCAATCCTGATGACCGAGAT-3′ (TfR reverse), 5′-TGACGGGGTCACC CAACTGTGCCCATCTA-3′(β- actin forward) and 5′-CTAGAAGCATTTGCGGTGGACG ATGGAGGG-3′. The qRT-PCR program was as follows: 95 °C for 3 min and 40 cycles of 95 °C for 15 s and 60 °C for 30 s. The amounts of TfR were normalized versus β-actin. Small RNA was isolated from HeLa and P19 cells using mirVana™ miRNA isolation kits (Ambion, USA), and then subjected to cDNA synthesis and qRT-PCR of mature miR9 using the mirVana™ qRT-PCR primer Set and the mirVana™ qRT-PCR miRNA kit (both from Ambion, USA). The qRT-PCR was performed in triplicate using an iCycer (Bio-Rad, USA) and SYBR Premix Ex Taq™ (2 × ; Takara, Japan) at 95 °C for 3 min and 40 cycles of 95 °C for 15 s

and 64 °C for 30 s. The relative amounts of miR9 were normalized versus the U6 snRNA primer set (Ambion, USA).

2.5. Iron uptake assays

HeLa and P19 cells were plated at 1 x 10^5 cells/well into 24well plates and cultured with Ferric Ammonium Citrate (FAC; 25 μM, Sigma, St Louis, MO) for 24 h before transfection. The cells, which was transfected with or without the CMV/TfR/3XPT_miR9, were washed with Phosphate Buffer Saline (PBS) and were counted by hematocytometer. These cells were then lysed with 100 μL/1 × 10^6 cells of 6 M HCl (Georgiachem, Seoul, Korea) after incubation at 70 °C for 30 min and the lysate was dilluted five times with distilled water. They were transferred into a 96-well plate (Chemicell GmbH, Germany) and, after addition of 5 μL of the iron color reagent in IRON/TIBC REAGENT SET (Pointe Scientific, INC., Canton, MI), the samples were incubated for 30 min at 37 °C. Before and after adding the reagent, the amount of iron uptake was analyzed by measuring the absorbance at 560 nm using SynergyMx (BiotEK, USA).

2.6. Fluorescence analysis

HeLa and P19 cells were treated with the MF targeting TfR or the MF-mt nanoparticles. 1 × 10^5 cells were treated with various concentrations of each nanoparticles. The cells were incubated with the nanoparticles at 4 °C for 30 min, and then washed two times for 10 min each at RT under mild shaking. These cells were lysed with RIPA buffer (Thermo Fisher Scientific Inc., Waltham, MA) and then transferred into dark 96-well plate (Chemicell GmbH, Germany) to measure the fluorescence intensity (50 μL) using SynergyMx (BiotEK, USA).

2.7. Magnetic resonance analysis

HeLa and P19 cells (5 × 10^5/well) treated with the MF targeting TfR or the MF-mt were washed with PBS three times and the cells were then detached by trypsin/ehtylenediaminetetraacetic acid (EDTA, invitrogen, Grand Island, NY). The detached cells were fixed with 4% paraformaldehyde and imaged using a 1.5 T clinical MRI Instrument with a micro-47 surface coil (Intera; Philips Medical Systems, Best, Netherlands). The T2-weighted MR images were measured using the Carr-Purcell-Meiboom-Gill (CPMG) sequence at room temperature under the following conditions: TR = 4000 ms, TE = 60 ms, slice thickness of 2.0 mm, resolution of 234 × 234 μm.

2.8. Confocal microscopy of the MF targeting TfR nanoparticles in HeLa and P19 cells

HeLa and P19 cells (1 × 10^5 cells/well) were seeded on 25-mm-diameter glass cover slips and grown for 24 h at 37 °C. Before treatment with the MF-mt and the MF targeting TfR, the cells were incubated for 30 min at 4 °C and then washed with PBS. The conjugated particles were added to cells under Tris buffer (pH 7). After incubation for 30 min at 4 °C, the cells were fixed by gently shaking for 20 min with a 4% formaldehyde solution (Sigma, St Louis, MO). Cells were then washed 3 times with PBS for 10 min and cover-slipped with mounting medium containing 4′, 6-diamidino-2-phenylindole dihydrochloride (DAPI) solution (Vector Laboratories, Inc., CA). The images were acquired using confocal laser scanning microscope (LSM 510; Carl Zeiss, Germany) at an excitation wavelength of 555 nm and an emission wavelength of 578 nm.

2.9. Immunofluorescence analysis of neuronal differentiation of P19 cells

P19 cells or matrigel incorporated into the P19 cells were fixed with 4% formaldehyde for 15 min, and then washed two times for 5 min with PBS, and gentle shaking was provided during incubation. The blocking and permeabilization procedures were performed simultaneously with 20% normal goat serum reaction mixture and 0.1% Triton X-100 for 60 min. The Oct-4 or Tuj1 protein was detected by a 1:1000 dilution of anti-Oct-4 antibody (Chemicon, Millipore, Watford, UK) or anti-Tuj1 antibody (Chemicon, Millipore, Watford, UK) and incubated overnight at 4 °C. After three washes for 5 min each, Alexa-488 and -594 Fluor secondary antibody conjugates were added and the mixture was incubated for 90 min. The P19 cells were placed on a cover slip and mounted with an aqueous mounting solution containing DAPI (Vector Laboratories, Inc., CA). The fluorescence signal was detected by confocal laser scanning microscopy (LSM 510; Carl Zeiss, Weimer, Germany).

2.10. In vivo fluorescence and MR imaging in nude mice

All animals used in the *in vivo* experiments were housed under specific pathogen-free conditions and the experiments were approved by institutional animal care and use committee in CHA University. The CMV/TfR/3XPT_miR9 was co-transfected into P19 cells with the CMV/Fluc. 1 × 10^6 cells were harvested in 150 μL of PBS and resuspended within 150 μL of matrigel. These cells were implanted into both thighs of a male Balb/c nude mice (7 weeks old; $n = 3$); the left thigh, without the RA treatment, was used as a control, and the right thigh was treated with RA for induction of neuronal differentiation. The MF targeting TfR (MF: 0.2 mg/150 μL) were injected into the mice via the tail vein. All mice received intraperitoneal injections of 70 μL of a Zoletil (Virbac, Carros, France) and Rompun (Bayer, Seoul, Korea) solution (2:1) for anesthesia. *In vivo* MR images were acquired using a 3T clinical MRI instrument with a micro-47 surface coil (Intera; Philips Medical Systems, Best, Netherlands). The T2-wieghted MR images were measured using the T2 Turbo Spin Echo sequence at room temperature with the following parameters: TR = 4000 ms, TE = 114 ms, slice thickness = 1.0 mm, FOV read = 180 mm. The *in vivo* fluorescence images were acquired using an IVIS spectrum (Xenogen, CA) and a red filter (605/30 nm, excitation filter; 660/20 nm, emission filter). A camera was used to acquire images at a constant exposure time (1 s). ROIs were drawn around the area of uptake in the right and left thighs on the IVIS images. The average counts per pixel were recorded for both thighs of the mouse. For *in vivo* bioluminescence imaging, 4 mg of D-luciferin for Fluc imaging was intraperitoneally injected and acquired the bioluminescence imaging by the IVIS spectrum (Xenogen, CA).

2.11. Statistical analysis

All data are presented as the means ± SD calculated from quadruple wells and significant differences between samples were assessed using a Student's *t*-test ($^*P < 0.05$).

3. Results

3.1. Design of the reverse complenetary multimodal imaging system to visualize miR9

To image endogenous miRNA-involved neurognesis using a reverse complementary multimodal imaging system, TfR regulated by a cytomegalovirus (CMV) promoter (CMV/TfR) was first selected and three copies of perfect complimentary target sequences against the mature miR9 (3XPT_miR9), which is highly expressed in the neuron, was cloned into the 3′ UTR of TfR (CMV/TfR/3XPT_miR9) as a miR9 TfR reporter gene (Fig. 1). Second, peptides targeting TfR were successfully conjugated to MF nanoparticles (MF targeting TfR) as a reverse complementary multimodal reporter probe for the CMV/TfR/3XPT_miR9. When the miR9 TfR reporter gene was transfected into cells, in the absence of miR9, TfR expression regulated by CMV promoter will increase and result in higher uptake of the MF targeting TfR nanoparticle in the cells. This high uptake of the MF nanoparticles will result in increased fluorescence signals and decreased MR signals simultaneously. In contrast, in the presence of miR9 in the cytoplasm of cells, the hybridization of miR9 with the target sequence within the miR9 TfR reporter gene will results in transcriptional repression of TfR and lower uptake of the reverse complementary multimodal reporter probes. This lower uptake of the MF targeting TfR nanoparticles will demonstrate low fluorescence signals and high MR signals simultaneously. In response to miR9 biogenesis, fluorescence signals of the MF targeting TfR nanoparticles will be represented as a signal-off system and in reverse, the MR signals of the MF targeting TfR nanoparticles will function as a signal-on imaging system. Therefore, this system will provide reverse complementary multimodal imaging information about miR9 biogenesis.

To synthesize the reverse complementary multimodal reporter probe, TfR peptides or a mutant were covalently conjugated to the MF nanoparsticle using the coupling reagent *N*-(3-dimethylaminopropyl)-*N*′-ethyl-carbodimide hydrochloride (EDC, 40 nmol) at a molar ration of 1:3. Transmission electron microscopy (TEM) demonstrated that all of the MF, MF mutant (MF-mt) and MF targeting TfR nanoparticles adopted a monospherical shape in aqueous solution (Fig. 2a). Dynamic light scattering (DLS) revealed that hydrodynamic particle diameters of the MF, MF-mt and MF targeting TfR nanoparticles were 55.9 ± 1.45 nm, 66.3 ± 0.37 nm and 138.1 ± 25.2 nm, respectively (Fig. 2b). These results indicated successful formation of the reverse complementary multimodal reporter probe.

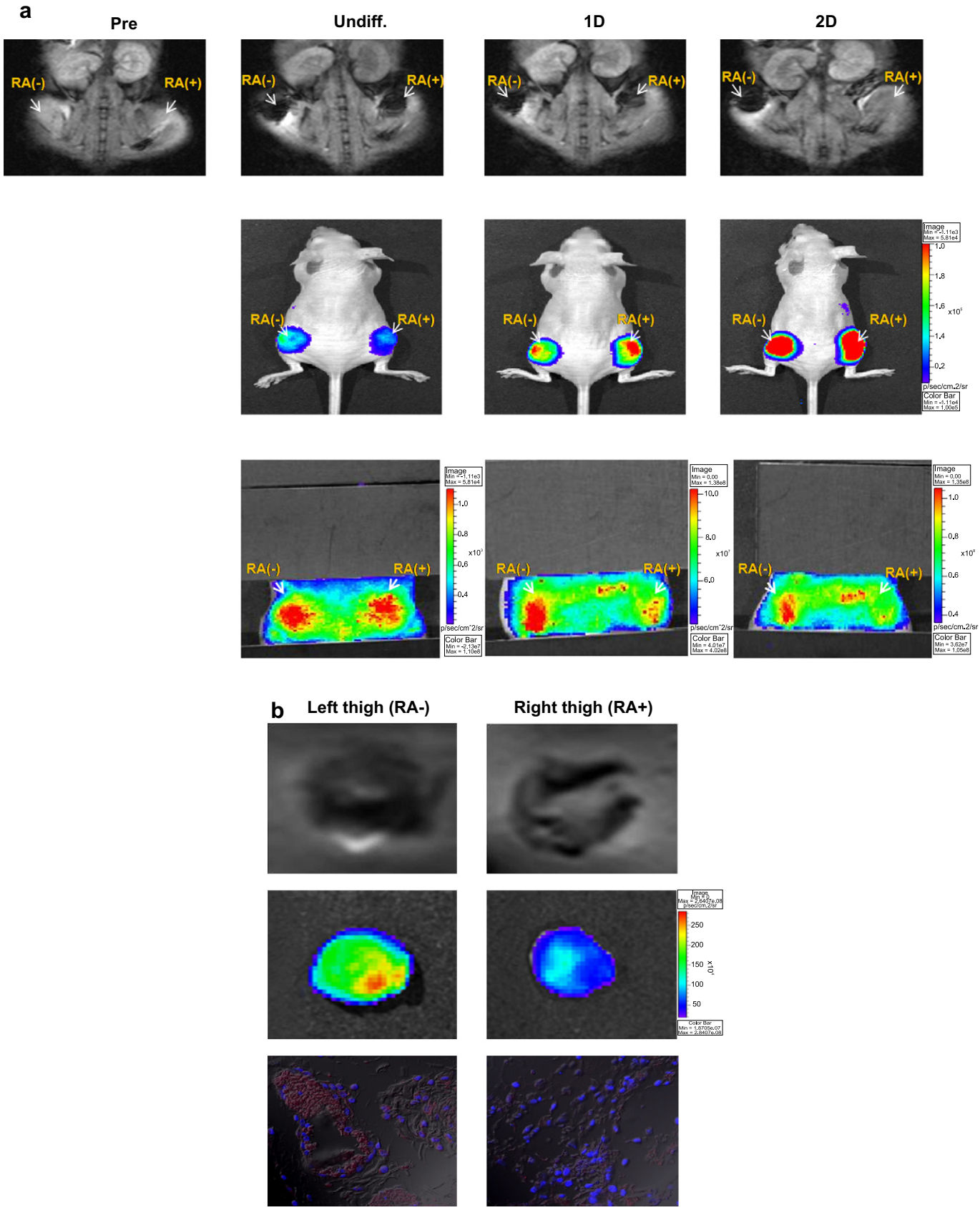

Fig. 5. *In vivo* reverse complementary multimodal imaging of miR9-involved neurogenesis of P19 cells. (a) P19 cells co-transfected with the CMV/TfR/3XPT_miR9 and the CMV/Fluc were incorporated into a prewetted matrigel. The P19 cell-incorporated matrigels treated either without (−) or with (+) RA for neuronal induction were implanted into the right thigh (white arrow) and left thigh (white arrow) of a nude mouse, respectively ($n = 3$). MR images (upper panel, 1.5T), bioluminescence images (middle panel) and fluorescence images (lower panel) were acquired for 2 days. MR images of the mouse bearing P19 cells without treatment of RA in the left thigh and with treatment of RA in the right thigh were acquired before and after IV

3.2. Reverse complementary imaging signals in fluorescence and MR intensities in response to miR9

To examine the specificity of the miR9 TfR reporter gene-based reverse complementary multimodal imaging in cells, we transfected HeLa cells (human cervical cancer cell line) with the CMV/TfR/3XPT_miR9. Compared with the P19 cells, which do not express miR9, qRT-PCR demonstrated no expression of endogenous miR9 and higher expression of endogenous TfR in HeLa cells (Fig. S1). In the absence of exogenous miR9, iron uptake significant increased in HeLa cells in a dose-dependent manner when the cells were transfected with 0, 1, 2 and 4 μg of the CMV/TfR/3XPT_miR9 due to the high expression of TfR, which is regulated by the CMV promoter (Fig. S2). In the absence of exogenous miR9, HeLa cells transfected with the CMV/TfR/3XPT_miR9 showed a significantly higher increase in fluorescence activity after treatment with the MF targeting TfR nanoparticles when compared with treatment of the MF-mt nanoparticles (Fig. 3a). In contrast, in the absence of miR9, T2-weighted MR images at 1.5T showed a gradual decrease in the magnetic signal intensity from HeLa cells transfected with the CMV/TfR/3XPT_miR9 as the concentration of the MF targeting TfR nanoparticles increased when compared with treatment of the MF-mt (Fig. 3b). Confocal microscopy images showed greater targeting specificity and fluorescence signals in the MF targeting TfR-treated HeLa cells transfected with the CMV/TfR/3XPT_miR9 than in the MF-mt-treated HeLa cells transfected with the CMV/TfR/3XPT_miR9 (Fig. 3c). Interestingly, HeLa cells transfected without the CMV/TfR/3XPT_miR9 showed a high increase in fluorescence activity and a high decrease in MR signals after treatment with the MF targeting TfR nanoparticles due to the high level of endogenous TfR in HeLa cells but the magnitude of both the fluorescence and MR signals was not higher and was not lower than the levels observed in HeLa cells transfected with the CMV/TfR/3XPT_miR9.

When exogenous miR9 was added, HeLa cells transfected with the CMV/TfR/3XPT_miR9 showed a significant decrease in iron uptake due to the repressed activity of TfR by hybridization of exogenous miR9 with the 3XPT in the miR9 TfR reporter gene, which resulted in the destabilization of TfR mRNA (Fig. S3). Similarly, as the concentration of the exogenous miR9 increased, confocal microscopy images demonstrated that the HeLa cells transfected with the CMV/TfR/3XPT_miR9 showed a significant decrease in uptake of the MF targeting TfR nanoparticles and a gradual decrease in fluorescence intensities and gradual increase in MR signals was observed due to the miR9 activity (Fig. 3d–f). Meanwhile, the addition of exogenous miR124a did not result in a decrease in the uptake of iron or MF targeting TfR nanoparticles in HeLa cells transfected with the CMV/TfR/3XPT_miR9 and no difference in fluorescence and MR intensities was observed as the concentration of miR124a increased. These results demonstrated the great specificity of the miR9 TfR reporter gene-based reverse complementary multimodal imaging system in response to miR9.

3.3. Increase in MR signals and decrease in fluorescence activities during miR9-involved neurogenesis of P19 cells

To image miR9-involved neurogenesis *in vivo* using the miR9 TfR reporter gene-based reverse complemetary multimodal imaging system, P19 cells were first selected and neuronal differentiation was induced by retinoic acid (RA). The undifferntiated P19 cells were verified using oct4 (stem cell marker) antibody, and morphological neurite outgrowth and immunofluorescence staining using Tuj1 (neuronal marker) antibody were clearly visualized 6 days after neuronal differentiation of the P19 cells (Fig. S4). The qRT-PCR analysis showed a significantly gradual increase in endogenous miR9 expression (Fig. 4a). Endogenous TfR expression both before and after induction of neuronal differentiation of the P19 cells was significantly lower than HeLa cells (Fig. 4b). However, only a slight decrease in endogenous TfR expression was observed between undifferentiated and differentiated P19 cells. Therefore, iron uptake was only slightly decreased after neuronal differentiation of the P19 cells (Fig. S5). When the CMV/TfR/3XPT_miR9 was transfected into undifferentiated and differentiated P19 cells, iron uptake was significantly and gradually decreased during neuronal differentiation. This occurred because miR9 gradually increases during neurogenesis of P19 cells, which resulted in a gradual decrease in the expression and functional activity of TfR from the CMV/TfR/3XPT_miR9 (Fig. S6). Meanwhile, for CMV/TfR-transfected P19 cells, which expressed constant TfR regardless of the presence of miR9, no significant difference in iron uptake between before and after neuronal differentiation of P19 cells was observed. Fluorescence brightness analysis of the confocal microscopy images demonstrated that a dramatic and gradual decrease in the uptake of MF targeting TfR nanoparticle occurred before and after neuronal differentiation of P19 cells transfected with the CMV/TfR/3XPT_miR9 due to the gradual increase in miR9 during neurogenesis (Fig. 4c). Quantitative fluorescence intensities from the MF targeting TfR-treated P19 cells showed a significantly gradual decrease during neurogenesis of P19 cells transfected with the CMV/TfR/3XPT_miR9 due to miR9-mediated gradual repression of TfR activity (Fig. 4d). In contrast, T2-weighted image showed a gradual increase in MR signals during neurogenesis of the MF targeting TfR-treated P19 cells transfected with the CMV/TfR/3XPT_miR9 due to gradually decreased uptake of the MF targeting TfR nanoparticles (Fig. 4e). Meanwhile, both MF-mt-treated P19 cells transfected with the CMV/TfR/3XPT_miR9 and MF targeting TfR-treated P19 cells without the transfection of the CMV/TfR/3XPT_miR9 showed no significant uptake of each nanoparticle inside the cells and no significant difference in fluorescence and MR signals before and after neurogenesis of 19 cells was observed due to the lack of targeting specificity of MF-mt and low endogenous level of TfR in P19 cells, respectively.

3.4. In vivo reverse complementary multimodal imaging of miR9-involved neurogenesis

To simultaneously monitor the decreased fluorescence signals and increased MR signals during neuronal differentiation of P19 cells using the miR9 TfR reporter gene-based reverse complementary multimodal imaging system *in vivo*, the miR9 TfR reporter gene was co-transfected into 1 x 10^6 P19 cells with a firefly luciferase (Fluc) reporter gene regulated by the CMV promoter (CMV/Fluc), which expresses a constant level of Fluc regardless of the presence of miR9 during neurogenesis. The P19 cells were cultured in a matrigel for *in vivo* imaging to reduce the false positive background MR signals inside the matrigel, which was observed as the white area of T2 MR scanning images [34,35]. The P19 cells-

injection of the MF targeting TfR nanoparticles. (b) Each matrigel implanted into both thighs of the nude mouse was isolated 2 days after placement of the P19 cell-incorporated matrigel. The upper panel showed a significant increase in T2-weighted MR signal from the right thigh treated with RA compared with the left thigh without the treatment of RA. Significantly decreased fluorescence signals (middle panel) was detected from the matrigel isolated from the right thigh compared with that from left thigh. Confocal microscopy images (lower panel, X400) of the slice sectioned from the left thigh showed a great fluorescence activity and uptake in the undifferentiated P19 cells compared to the fluorescence signals in the slice of the right thigh.

incorporated matrigels were then subcutaneously implanted into both thighs of a nude mouse. Only the cell–matrigel complex implanted into right thigh was induced to undergo neuronal differentiation. The internal control of the CMV/Fluc demonstrated that Fluc signals did not differ between undifferentiated P19 cells in left thigh and differentiated P19 cells in right thigh during 2 days, implying that equal number of cells were implanted and survived in both thighs for 2 days (Fig. 5a, middle panel, $n = 3$). The MF targeting TfR nanoparticles were systematically administered into the mouse bearing the P19 cell-incorporated matrigel in both thighs and reverse complementary imaging was acquired over 2 days. Since it was a challenge to obtain high quality *in vivo* fluorescence images because of the high autofluorescence backgrounds, the animals were shielded to scrutinize the area where the P19 cells-incorporated matrigel was located. The fluorescence signals were gradually decreased from the right thigh of the mouse treated with RA for induction of miR9-involved neurogenesis due to the gradually increase of miR9 in the differentiated P19 cells when compared with the left thigh that was not treated with RA (Fig. 5a, lower panel). In the T2-weighted MR images of the same mouse, dark signals were clearly visualized in both thighs containing the P19 cell-incorporated matrigel 0 days after intravenous (IV) injection of the MF targeting TfR nanoparticles when compared with pre-injection of the MF targeting TfR nanoparticles (Fig. 5a, upper panel). However, the brightness of the T2-weighted MR image from the right thigh progressively increased during neuronal differentiation. This was attributed to the gradual increase in T2-weighted MR signals due to the progressive increase in miR9 expression during neurogenesis of P19 cells. Meanwhile, no significant change in the T2-weighted MR signals was observed from the left thigh over 2 days.

The implanted P19 cell-incorporated matrigels from both thighs were carefully isolated 2 days after IV injection of the MF targeting TfR nanoparticles to confirm whether *in vivo* flurorescence and MR imaging for miR9-involved neurogenesis were acquired by the reverse complementary multimdoal reporter probe. A brighter and higher T2 MR signal was detected in the matrigel incorporating post-differentiated P19 cells when compared with the undiffrentiated P19 cell-incorporated matrigel (Fig. 5b, upper panel). Quantitative region of interest (ROI) showed approximately 2-fold increase in MR signals from the differentiated P19 cell-incorporating matrigel relative to the MR signals from the pre-differentiated P19 cell-incorporating matrigel (Fig. S7). The matrigel isolated from the right thigh had about a 2-fold lower fluorescence intensity (Fig. 5b, middle panel and Fig. S8). In addition, the fluorescence activity of the frozen sections isolated from the differentiated P19 cell-incorporating matrigel showed much lower uptake of MF targeting TfR nanoparticles than the pre-differentiated P19 cell-incorporating matrigel, which corresponded to the high MR and low fluorescence signals in the right thigh (Fig. 5b, lower panel). Immunohistochemical staining using the Tuj1 antibody demonstrated that the flurosrescence signals was only in the P19 cells isolated from the right thigh, while fluorescence activity using the Oct4 antibody was only observed in the P19 cells isolated from the left thigh, implying that low uptake of MF targeting TfR nanoparticle in the RA-treated right thigh was due to the miR9-involved neurogenesis of P19 cells, which resulted in the high MR signal and low fluorescence signals (Fig. S9).

4. Discussion

Many molecular imging systems, inclduing nanoparticle-based multimodal imaging systems, have been developed for targeting of extracellular molecules and diagnosis of cancers [25,36,37]. Multimodal imaging systems can offer the benefits of complementary modalities that may eliminate the disadvantages of individual imaging modalities by providing complementary information about cellular and molecular activites. However, little work has been directed at developing a multimodal imaging system to detect and monitor cellular differentiation and intracellular gene activity. Recently, intracellularly expressed miRNAs have been reported to be related to cell developments and various diseases, including cancer and neurological disease [38]. Molecular imaging of miRNAs are very important in disease diagnosis and miRNA-related cellular therapy. We have recently developed a systemt to image intracellularly expressed miRNAs using a bioluminescent reporter gene and fluorescent molecular beacon and this approach has been successfully used for *in vivo* imaging of miRNA-invovled cellular development processes [16,17,21–23,39]. However, both optical miRNA imaging systems have limitations in regards to clinical application due to signal-off imaging, safety and depth penetration.

In this study, we developed a reverse complementary multimodal imaging system which could provide signal-on multimodal visualization for miRNA biogenesis and cellular development processes. The expression and functional activity of TfR from the miR9 TfR reporter gene were successfully regulated by miR9 during neurogenesis. In the absence or even low expression of miR9, peptides of the MF targeting TfR nanoparticles successfully targeted TfR, which are highly expressed in the cellular membrane, and were internalized into P19 cells. During neuronal differentiation of P19 cells, only low levels of the MF targeting TfR nanoparticles were targeted and internalized into P19 cells because miR9 is highly expressed during neurogenesis of P19 cells, which results in great decrease in the expression and functional activity of TfR from the CMV/TfR/3XPT_miR9. The miR9 expression-inversely dependent uptake of MF targeting TfR nanoparticles was well visualized during pre-differentiation of P19 cells and a high fluorescence and low MR signals were observed. In contrast, during post-differentiation of P19 cells, low fluorescence and high MR signals were observed. Therefore, the miR9 TfR reporter gene-based reverse complementary multimodal imaging system for miR9-involved neurogenesis demonstrated that the fluorescence activities were a signal-off system, whereas the MR signals functioned as a signal-on imaging system. However, high quality *in vivo* image could not be readily obtained using the the fluorescence imaging dye, RITC, due to the relatively short emission wavelength of the dye molecules. Thus, a combination of near-infrared fluorescence dyes with MR nanoparticles will be used in the development of an alternative for *in vivo* imaging. In addition, *in vivo* reverse complementary multimodal imaging of miR9-involved neurogenesis of P19 cells 3 days after the implantation of P19 cells into the nude mouse could not be achieved due to the transient transfection of the miR9 TfR reporter gene into P19 cells. Thus, for long-term imaging of miRNA-involved neurogenesis using the reverse complementary multimodal imaging system, cell lines stably expressing the miRNA TfR reporter gene should be used to overcome this limitation.

This is the first *in vivo* MR imaging system that has been developed to image miRNA expression and neurogenesis. It is also the first documented attempt to image miRNA using a reverse complementary multimodal nanoparticle. The application of the miRNA TfR reporter gene-based reverse complementary multimodal imaging system will offer many benefits to noninvasively study the expression and function of miRNAs in relation to cellular development, including proliferation, apoptosis and differentiation, and diseases, such as cancer, diabetes and neurological diseases [3–12,40]. Unlike the existing MR imaging reagents, it will be

a useful tool for *in vivo* cellular tracking as well as for monitoring *in vivo* cellular development with anatomical imaging.

5. Conclusion

We have successfully developed a reverse complementary multimodal imaging system to visualize miR9-involved neurogenesis *in vitro* and *in vivo*. In response to miR9 expression during neurogenesis of P19 cells, this system demonstrated that fluorescence activity was represented as a signal-off system, in reverse complement, MR signals as a signal-on system. The reverse complementary multimodal imaging system can be used as a new miRNA imaging probe for the real-time monitoring of miRNA-related cellular differentiation and disease processes through repetitive imaging of the same animal.

Acknowledgments

This work was supported by a grant of the Korea Healthcare technology R&D Project, Ministry for Health, Welfare & Family Affairs, Republic of Korea (A085136 and A100377), National Research Foundation of Korea (No. 2011-0027482) and the Bio & Medical Technology Development Program of the National Research Foundation (NRF) funded by the Korean government (MEST) (No. 2012-0006097).

Appendix A. Supplementary data

Supplementary data related to this article can be found online at doi:10.1016/j.biomaterials.2012.05.057.

References

[1] Bartel DP. MicroRNAs: target recognition and regulatory functions. Cell 2009; 136:215–33.
[2] Hutvagner G, Zamore PD. A microRNA in a multiple-turnover RNAi enzyme complex. Science 2002;297:2056–60.
[3] Zeng Y, Yi R, Cullen BR. MicroRNAs and small interfering RNAs can inhibit mRNA expression by similar mechanisms. Proc Natl Acad Sci USA 2003;100: 9779–84.
[4] Brennecke J, Hipfner DR, Stark A, Russell RB, Cohen SM. Bantam encodes a developmentally regulated microRNA that controls cell proliferation and regulates the proapoptotic gene hid in Drosophila. Cell 2003;113:25–36.
[5] Xu P, Vernooy SY, Guo M, Hay BA. The Drosophila microRNA Mir-14 suppresses cell death and is required for normal fat metabolism. Curr Biol 2003;13:790–5.
[6] Dostie J, Mourelatos Z, Yang M, Sharma A, Dreyfuss G. Numerous microRNPs in neuronal cells containing novel microRNAs. RNA 2003;9:180–6.
[7] Kloosterman WP, Plasterk RH. The diverse functions of microRNAs in animal development and disease. Dev Cell 2006;11:441–50.
[8] Weiler J, Hunziker J, Hall J. Anti-miRNA oligonucleotides (AMOs): ammunition to target miRNAs implicated in human disease? Gene Ther 2006;13:496–502.
[9] Zamore PD, Haley B. Ribo-gnome: the big world of small RNAs. Science 2005; 309:1519–24.
[10] Sullivan CS, Ganem D. MicroRNAs and viral infection. Mol Cell 2005;20:3–7.
[11] Croce CM, Calin GA. MiRNAs, cancer, and stem cell division. Cell 2005;122: 6–7.
[12] Iorio MV, Croce CM. MicroRNAs in cancer: small molecules with a huge impact. J Clin Oncol 2009;27:5848–56.
[13] Smirnova L, Grafe A, Seiler A, Schumacher S, Nitsch R, Wulczyn FG. Regulation of miRNA expression during neural cell specification. Eur J Neurosci 2005;21: 1469–77.
[14] Krichevsky AM, King KS, Donahue CP, Khrapko K, Kosik KS. A microRNA array reveals extensive regulation of microRNAs during brain development. RNA 2003;9:1274–81.
[15] Deo M, Yu JY, Chung KH, Tippens M, Turner DL. Detection of mammalian microRNA expression by in situ hybridization with RNA oligonucleotides. Dev Dyn 2006;235:2538–48.
[16] Ko MH, Kim S, Hwang do W, Ko HY, Kim YH, Lee DS. Bioimaging of the unbalanced expression of microRNA9 and microRNA9* during the neuronal differentiation of P19 cells. FEBS J 2008;275:2605–16.
[17] Lee JY, Kim S, Hwang do W, Jeong JM, Chung JK, Lee MC, et al. Development of a dual-luciferase reporter system for in vivo visualization of MicroRNA biogenesis and posttranscriptional regulation. J Nucl Med 2008;49:285–94.
[18] Kim HJ, Chung JK, Hwang do W, Lee DS, Kim S. In vivo imaging of miR-221 biogenesis in papillary thyroid carcinoma. Mol Imaging Biol 2009;11:71–8.
[19] Kim HJ, Kim YH, Lee DS, Chung JK, Kim S. In vivo imaging of functional targeting of miR-221 in papillary thyroid carcinoma. J Nucl Med 2008;49: 1686–93.
[20] Ko HY, Hwang do W, Lee DS, Kim S. A reporter gene imaging system for monitoring microRNA biogenesis. Nat Protoc 2009;4:1663–9.
[21] Hwang do W, Song IC, Lee DS, Kim S. Smart magnetic fluorescent nanoparticle imaging probes to monitor microRNAs. Small;6:81–88.
[22] Kang WJ, Cho YL, Chae JR, Lee JD, Choi KJ, Kim S. Molecular beacon-based bioimaging of multiple microRNAs during myogenesis. Biomaterials 1915–22;32.
[23] Kim JK, Choi KJ, Lee M, Jo MH, Kim S. Molecular imaging of a cancer-targeting theragnostics probe using a nucleolin aptamer- and microRNA-221 molecular beacon-conjugated nanoparticle. Biomaterials;33:207–217.
[24] Weissleder R, Moore A, Mahmood U, Bhorade R, Benveniste H, Chiocca EA, et al. In vivo magnetic resonance imaging of transgene expression. Nat Med 2000;6:351–5.
[25] Moore A, Josephson L, Bhorade RM, Basilion JP, Weissleder R. Human transferrin receptor gene as a marker gene for MR imaging. Radiology 2001;221: 244–50.
[26] Gilad AA, Ziv K, McMahon MT, van Zijl PC, Neeman M, Bulte JW. MRI reporter genes. J Nucl Med 2008;49:1905–8.
[27] Bulte JW, Douglas T, Witwer B, Zhang SC, Strable E, Lewis BK, et al. Magnetodendrimers allow endosomal magnetic labeling and in vivo tracking of stem cells. Nat Biotechnol 2001;19:1141–7.
[28] Zhang RL, Zhang L, Zhang ZG, Morris D, Jiang Q, Wang L, et al. Migration and differentiation of adult rat subventricular zone progenitor cells transplanted into the adult rat striatum. Neuroscience 2003;116:373–82.
[29] Cohen B, Dafni H, Meir G, Harmelin A, Neeman M. Ferritin as an endogenous MRI reporter for noninvasive imaging of gene expression in C6 glioma tumors. Neoplasia 2005;7:109–17.
[30] Cohen B, Ziv K, Plaks V, Israely T, Kalchenko V, Harmelin A, et al. MRI detection of transcriptional regulation of gene expression in transgenic mice. Nat Med 2007;13:498–503.
[31] Ichikawa T, Hogemann D, Saeki Y, Tyminski E, Terada K, Weissleder R, et al. MRI of transgene expression: correlation to therapeutic gene expression. Neoplasia 2002;4:523–30.
[32] Wangler C, Nada D, Hofner G, Maschauer S, Wangler B, Schneider S, et al. In vitro and initial in vivo evaluation of (68)Ga-labeled transferrin receptor (TfR) binding peptides as potential carriers for enhanced drug transport into TfR expressing cells. Mol Imaging Biol;13:332–341.
[33] Hwang do W, Ko HY, Lee JH, Kang H, Ryu SH, Song IC, et al. A nucleolin-targeted multimodal nanoparticle imaging probe for tracking cancer cells using an aptamer. J Nucl Med;51:98–105.
[34] Kang HW, Torres D, Wald L, Weissleder R, Bogdanov Jr AA. Targeted imaging of human endothelial-specific marker in a model of adoptive cell transfer. Lab Invest 2006;86:599–609.
[35] Deramaudt TB, Takaoka M, Upadhyay R, Bowser MJ, Porter J, Lee A, et al. N-cadherin and keratinocyte growth factor receptor mediate the functional interplay between Ki-RASG12V and p53V143A in promoting pancreatic cell migration, invasion, and tissue architecture disruption. Mol Cell Biol 2006;26: 4185–200.
[36] Ray P, De A, Min JJ, Tsien RY, Gambhir SS. Imaging tri-fusion multimodality reporter gene expression in living subjects. Cancer Res 2004;64:1323–30.
[37] Lee HY, Li Z, Chen K, Hsu AR, Xu C, Xie J, et al. PET/MRI dual-modality tumor imaging using arginine-glycine-aspartic (RGD)-conjugated radiolabeled iron oxide nanoparticles. J Nucl Med 2008;49:1371–9.
[38] Lim LP, Lau NC, Garrett-Engele P, Grimson A, Schelter JM, Castle J, et al. Microarray analysis shows that some microRNAs downregulate large numbers of target mRNAs. Nature 2005;433:769–73.
[39] Ko HY, Lee DS, Kim S. Noninvasive imaging of microRNA124a-mediated repression of the chromosome 14 ORF 24 gene during neurogenesis. FEBS J 2009;276:4854–65.
[40] Bartel DP. MicroRNAs: genomics, biogenesis, mechanism, and function. Cell 2004;116:281–97.